Neutron Diffraction of Homopolyatomic Bismuth Ions in Liquid $Bi_5(AlCl_4)_3$ and ab Initio Study of the Structure and Bonding of the Isolated Bi_5^{3+} Ion

Kazuhiko Ichikawa,* Tetsuo Yamanaka, and Atsushi Takamuku

Division of Material Science, Graduate School of Environmental Earth Science, Hokkaido University, Sapporo 060, Japan

Rainer Glaser*

Department of Chemistry, University of Missouri−Columbia, Columbia, Missouri 65211

Received May 22, 1997[⊗]

Time-of-flight neutron diffraction measurements were carried out at 350 °C and 450 ± 5 °C for molten $Bi_5(AlCl_4)_3$. Contributions from $AlCl_4^-$ were estimated using molten $LiAlCl_4$ data and yielded radial distribution functions $RDF^{rem}(r)$ that allowed for the determination of the D_{3h}-Bi_5^{3+} structure: $d(Bi_a-Bi_e) = 3.2$ Å and $d(Bi_e-Bi_e) = 3.4$ Å. The functions $RDF^{rem}(r)$ were simulated successfully by a model of intermediate range order similar to the environment in $Bi_5(AlCl_4)_3$ crystals. The first sharp diffraction peak (FSDP) occurs at ca. 1.2 $Å^{-1}$ and suggests a distance between Bi_5^{3+} and $AlCl_4^-$ ions of about 5.5 Å in close agreement with values for the solid (5.6−6.2 Å). The free D_{3h}-Bi_5^{3+} ion was studied with RHF, MP2, and QCISD(T) methods. Effective core potentials were used in conjunction with polarized split-valence LANL1DZ basis sets. At the QCISD(T)/LANL1DZ+PP level, distances of $d(Bi_a-Bi_e) = 3.073$ Å and $d(Bi_e-Bi_e) = 3.331$ Å were determined. The Bi_a-Bi_e distances consistently are shorter by about $\Delta(Bi-Bi) = 0.26$ Å in the free ion, by ca. 0.3 Å in $Bi_5(AlCl_4)_3$ crystals, and by ca. 0.2_5 Å in the liquid. Natural population analysis shows a larger charge on Bi_a (+0.74) than on Bi_e (+0.51). Natural electron configuration analyses show intact 6s-type Bi lone pairs. The lowest-lying cluster MOs are a_1' (radial), e″ (mixed), a_2'' (∥), and e′(⊥), and they are illustrated via contour plots of partial electron density functions. The molecular graph of Bi_5^{3+} shows compelling evidence for strong bonding along all edges.

Introduction

Bismuth possesses a number of unusually low oxidation states below the familiar Bi(III). In fact, bismuth has become *the* classical example of an element forming a series of homopolyatomic ions. Early investigations were concerned mainly with dilute solutions of bismuth metal in $BiCl_3$ melts.[1−4] The results of EMF and spectroscopic studies on these melts are consistent with the presence of Bi^+, Bi_3^+, and Bi_4^{4+}. The solid-phase $Bi_{24}Cl_{28}$ has been shown by X-ray diffraction studies to be $(Bi_9^{5+})_2(BiCl_5^{2-})_4(Bi_2Cl_8^{2-})$.[5,6] These complex ions of bismuth chloride were studied by Raman spectroscopy.[7,8] The lower oxidation states of bismuth, such as the ones represented by the entities Bi_5^{3+}, Bi_8^{2+}, and Bi_9^{5+}, were characterized by spectroscopic cyclic voltammogram measurements in molten acidic chloroaluminate melts of the $AlCl_3$ + NaCl eutectic and the 2:1 $AlCl_3$ + *N*-(*n*-butyl)pyridinium chloride.[9−11]

The solid phases $Bi_5(AlCl_4)_3$ and $Bi_8(AlCl_4)_2$ were isolated from the pseudobinary system $Bi-(BiCl_3+AlCl_3)$.[12−14] A material with composition $Bi_{10}Hf_3Cl_{18}$ was prepared to explore the effects of a large cation of relatively high stability.[15] An X-ray diffraction study of the system $Bi-(2BiCl_3+3HfCl_4)$ showed, however, that the composition of this compound is $(Bi_9^{5+})(Bi^+)(HfCl_6^{2-})_3$ and not $(Bi_5^{3+})_2(HfCl_6^{2-})_3$. The vibrational modes of the Bi_5^{3+} ion were investigated by infrared or Raman spectroscopy.[7] More recently the full single-crystal analysis of $Bi_5(AlCl_4)_3$ including the intramolecular structure of the Bi_5^{3+} ion was reported.[14]

The interesting bonding of the homopolyatomic ion in $Bi_5(AlCl_4)_3$ was first discussed by Corbett in 1968.[12] Corbett asked "whether it should be possible to predict the configuration of the electron-poor ion Bi_5^{3+} based on simple bonding considerations" and employed MO arguments in an attempt at an answer. The large 6s−6p and 6p−6d separations were taken to allow for an iso-orbital treatment in terms of the 6p orbitals only and with the 6s electrons being considered part of the Bi core. Corbett's LCAO−MO calculations show that the D_{3h} symmetric trigonal bipyramid results in bonding MOs of a_1', a_2'', e′, and e″ symmetry and these are fully occupied by the 12 valence electrons and are well separated from the antibonding e′ LUMO. The square pyramid structure was dismissed because this system would require 14 electrons to occupy all bonding

[⊗] Abstract published in *Advance ACS Abstracts,* October 15, 1997.

(1) Yosim, S. J.; Darnell, A. J.; Gehman, W. G.; Mayer, S. W. *J. Phys. Chem.* **1959**, *63*, 230.
(2) Topol, L. E.; Yosim, S. J.; Osteryoung, R. A. *J. Phys. Chem.* **1961**, *65*, 1511.
(3) Boston, C. R.; Smith, G. P.; Howick, L. C. *J. Phys. Chem.* **1963**, *67*, 1849.
(4) Corbett, J. D.; Alber, F. C.; Sallach, R. A. *Inorg. Chim. Acta* **1968**, *2*, 22.
(5) Hershaft, A.; Corbett, J. D. *Inorg. Chem.* **1963**, *2*, 979.
(6) Friedman, R. M.; Corbett, J. D. *Inorg. Chim. Acta* **1973**, *7*, 525.
(7) Burns, R. C.; Gillespie, R. J.; Luk, W.-C. *Inorg. Chem.* **1978**, *17*, 3596.
(8) Ichikawa, K.; Fukushi, K. *J. Raman Spectrosc.* **1986**, *17*, 139.
(9) Bjerrum, N. J.; Boston, C. R.; Smith, G. P. *Inorg. Chem.* **1967**, *6*, 1162.
(10) Bjerrum, N. J.; Smith, G. P. *Inorg. Chem.* **1967**, *6*, 1968.
(11) Heerman, L.; D'Olieslager, W. *J. Electrochem. Soc.* **1991**, *138*, 1372.
(12) Corbett, J. D. *Inorg. Chem.* **1968**, *7*, 198.
(13) Krebs, B.; Hucke, M.; Brendel, C. J. *Angew. Chem., Int. Ed. Engl.* **1982**, *21*, 445.
(14) Krebs, B.; Mummert, M.; Brendel, C. *J. Less-Common Met.* **1986**, *116*, 159.
(15) Friedman, R. M.; Corbett, J. D. *Inorg. Chem.* **1973**, *12*, 1134.

S0020-1669(97)00608-3 CCC: $14.00

Chart 1. Regular Trigonal Bipyramid of Bi_5^{3+} with D_{3h} Symmetry

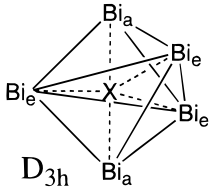

MOs and because the binding energy for this arrangement would also be less.[16] The valence electron count for Bi_5^{3+} (22 electrons) fits the polyhedral skeletal electron pair[17] approach for *closo* deltahedra with 4n+2 electrons. The Bi_5^{3+} ion was studied with extended Hückel theory,[18] and Ulvenlund et al.[19] recently reported results of ab initio calculations. The structure of D_{3h}-Bi_5^{3+} was optimized using RHF, MP2, and CISD theory and several types of effective core potentials were employed in conjunction with singly-polarized valence basis sets (d-exponent 0.17). Mulliken populations indicated charges of +0.72 for Bi_a and +0.52 for Bi_e, respectively, and the reported Mulliken overlap populations indicated reasonably strong equatorial and axial bonds.[19]

In this paper, we report the results of a neutron diffraction measurement of the intramolecular structure of the D_{3h}-symmetric Bi_5^{3+} (Chart 1) ion in the liquid state. The usual diffraction techniques in crystal and liquid states unfortunately do not have sufficiently high resolution, and reliable experimental electron density distributions cannot be determined. Theoretical methods are therefore particularly valuable to determine and to study electron density distributions, and we have studied the structure and the electronic structures of the homopolyatomic bismuth ion Bi_5^{3+} with various quantum-mechanical methods including the highly correlated quadratic CI level QCISD(T) in conjunction with effective core potentials and well-polarized basis sets. The electron density distribution has been explored with Weinhold's natural bond orbital (NBO) methods[20] to derive natural populations and to determine natural electron configurations. The cluster molecular orbitals are illustrated via contour plots of partial electron density functions determined from the ab initio wave function. These molecular orbitals can be readily understood as the result of LCAO of radial and tangential Bi p-type atomic orbitals. The bonding has been characterized with Bader's topological method, and the molecular graph shows compelling evidence for strong bonding along all edges of the Bi_5^{3+} ion.[21]

Neutron Diffraction Theory and Experimental Section

Neutron Diffraction Theory. The observed total scattering cross section taken from the neutron diffraction experiment is divided into self and interference terms as follows:

$$(d\sigma/d\Omega)_{total} = (d\sigma/d\Omega)_{int} + (d\sigma/d\Omega)_{self} \quad (1)$$

The self term scaled for a molecule formulated as $Bi_x(AlCl_4)_{1-x}$ can be written as

$$(d\sigma/d\Omega)_{self} = x\sigma_{s,Bi}/4\pi + (1-x)(\sigma_{s,Al} + 4\sigma_{s,Cl})/4\pi \quad (2)$$

where x is equal to 0.625 for the compound $Bi_5(AlCl_4)_3$; $\sigma_{s,i}$ denotes the total scattering cross section of nucleus i. The interference term can be divided into the two contributions from the intramolecular part for a complex ion of $AlCl_4^-$ (T_d) and the remaining part

$$(d\sigma/d\Omega)_{int} = (d\sigma/d\Omega)_{int}^{rem} + (d\sigma/d\Omega)_{int}^{intra} \quad (\text{for } AlCl_4^-) \quad (3)$$

The intramolecular interference term, the scattering from $AlCl_4^-$ (T_d), can be expressed as

$$(d\sigma/d\Omega)_{int}^{intra} = (1-x)\{8b_{Al}b_{Cl}\exp(-l_{AlCl}^2Q^2/2) \times \sin(Qr_{AlCl})/Qr_{AlCl} + 12b_{Cl}^2\exp(-l_{ClCl}^2Q^2/2)\sin(Qr_{ClCl})/Qr_{ClCl}\} \quad (4)$$

where r_{ij} and l_{ij} denote the internuclear distance and the root-mean-square amplitude of the nuclear pair i−j, respectively. The remaining interference term is given by

$$(d\sigma/d\Omega)_{int}^{rem} = x^2b_{Bi}^2[a_{BiBi}(Q)-1] + x(1-x)\{2b_{Bi}b_{Al}[a_{BiAl}(Q)-1] + 8b_{Bi}b_{Cl}[a_{BiCl}(Q)-1]\} + (1-x)^2\{b_{Al}^2[a_{AlAl}(Q)-1] + 8b_{Al}b_{Cl}[a_{AlCl}(Q)-1] + 16b_{Cl}^2[a_{ClCl}(Q)-1]\} \quad (5)$$

Here the partial structure factors a_{AlCl}, a_{ClCl}, and a_{AlAl} do not include contributions from the intramolecular interference of $AlCl_4^-$. The values b_{Bi}, b_{Cl}, and b_{Al} of the neutron scattering length are equal to 8.5256, 9.58, and 3.45 fm. The Fourier transform of $(d\sigma/d\Omega)_{int}$ and $(d\sigma/d\Omega)_{int}^{rem}$ gives the radial distribution functions as follows:

$$RDF(r) = (2r/\pi\Delta)\int (d\sigma/d\Omega)_{int}Q\sin(Qr)\,dQ + 4\pi\rho r^2 \quad (6)$$

and

$$RDF^{rem}(r) = (2r/\pi\Delta)\int (d\sigma/d\Omega)_{int}^{rem}Q\sin(Qr)\,dQ + 4\pi\rho r^2 \quad (7)$$

where $\Delta = [xb_{Bi} + (1-x)(b_{Al} + 4b_{Cl})]^2$ and ρ stands for the number density of $Bi_x(AlCl_4)_{1-x}$ where $x = 0.625$. In $RDF^{rem}(r)$ we cannot see any peaks at the intramolecular distances of r_{AlCl} and r_{ClCl} in $AlCl_4^-$.

Materials. Bismuth trichloride was purified by vacuum distillation. Bismuth metal is 99.9997% pure. A completely colorless single crystal of aluminum trichloride was used. Solid $Bi_5(AlCl_4)_3$ was prepared by fusion of stoichiometric quantities of $BiCl_3$, $AlCl_3$, and Bi. The manipulations were performed under an argon atmosphere in a glovebox. The sample of $Bi_5(AlCl_4)_3$ was sealed under vacuum into quartz cells (0.502 cm^2 cross section and 0.4 mm thickness) for the time-of-flight neutron diffraction measurements.

Time-of-Flight Neutron Diffraction Measurements. The time-of-flight neutron diffraction measurements were carried out at 350 and 450 ± 5 °C using the HIT spectrometer installed at the neutron source at KENS, Japan. The neutron diffraction measurements of molten $Bi_5(AlCl_4)_3$ were carried out for ca. 10 h. The measurements were also made for a vanadium rod of 8 mm diameter, an empty, and a blank.

Quantum-Mechanical Methods and Computational Section

Theoretical Methods. Restricted Hartree−Fock theory (RHF) was employed and electron correlation effects were included using second-order Mϕller−Plesset (MP2) perturbation theory[22] and QCISD(T)

(16) The C_{2v} structure does in fact correspond to a saddle point and Jahn−Teller distorts to a local minimum which is energetically well above the D_{3h} structure. Full details of the potential energy surface analysis will be disclosed elsewhere.

(17) Mingos, D. M. P. *Acc. Chem. Res.* **1984**, *17*, 311.
(18) Burns, R. C.; Gillespie, R. J.; Barnes, J. A.; McGlinchey, J. *Inorg. Chem.* **1982**, *21*, 799.
(19) Ulvenlund, S.; Ståhl, K.; Bengtsson-Kloo, L. *Inorg. Chem.* **1996**, *35*, 223.
(20) (a) Carpenter, J. E.; Weinhold, F. *J. Mol. Struct. (THEOCHEM)* **1988**, *169*, 41. (b) Curtiss, L. A.; Pochatko, D. J. *J. Chem. Phys.* **1985**, *82*, 2679. (c) Arnaud, R. *J. Comput. Chem.* **1994**, *15*, 1341.
(21) Bader, R. F. W. *Atoms in Molecules. A Quantum Theory*; Oxford University Press: New York, 1990.
(22) (a) Frisch, M. J.; Head-Gordon, M.; Pople, J. A. *Chem. Phys. Lett.* **1990**, *166*, 275. (b) Head-Gordon, M.; Head-Gordon, T. *Chem. Phys. Lett.* **1994**, *220*, 122.

theory.[23] The quadratic configuration interaction (QCI) method consists of a CI method that restores size consistency. If the QCI calculations are carried out in the space of the single and double excitations, the method is denoted QCISD and is equivalent to the coupled-cluster method CCSD.[24] Triple substitutions can be included as a perturbation to the QCISD solution, and the energy thus obtained is denoted QCISD(T).[25] In the largest effective core potential calculations, the active space comprised all of the 65 MOs generated by the basis functions for the 6s and 6p valence electrons and by the polarization functions of the five Bi atoms.

In the ground state configuration of bismuth, ^{4}S, the 83 electrons are distributed according to KLMN5s(2)5p(6)5d(10)6s(2)6p(3). Because of the large number of electrons of the ion, we employed effective core potentials in conjunction with different basis sets for the valence electrons.[26] At the LANL1DZ level, all of the electrons associated with shells K through O ($n = 1-5$) are replaced by effective core potentials. The remaining 6s and 6p orbitals are described by a split-valence basis set of 21-quality; that is, each orbital is described by one inner basis function constructed by contraction of two primitive Gaussian functions, and the outer basis function is described by a single flat Gaussian function. This valence basis set can be improved by the addition of sets of polarization functions. We have added sets of five d-functions to each Bi atom with d-exponent 0.185 as suggested by Huzinaga.[27a] The resulting polarized basis set is denoted LANL1DZ+P.[28] The addition of two sets of such d-functions with different d-exponents effectively results in the optimization of the d-exponent. We explored the consequences of optimization of the d-exponent with the basis set LANL1DZ+PP which contains two sets of d-functions with exponents 0.069 and 0.229 on each Bi atom. Ulvenlund et al.[19] preferred the basis set by Stevens and co-workers[29] (denoted SKBJ*) which they thought to perform best in comparison to experimental data. It must be noted, however, that their evaluation of basis sets was carried out at the RHF and MP2 levels and their more complete correlation treatment at the CISD level employed only the SKBJ* basis set. Our results will show (*vide infra*) that the Los Alamos basis sets perform very well when augmented with polarization functions and when higher-level correlation treatments, such as QCISD(T), are employed.

The topological electron density analysis was carried out with an all-electron basis set. Several all-electron basis sets for Bi are available,[27b] and one of these consists of a (3333333/33333/333/4) basis set in which s-, p-, and d-functions all are described by one basis function resulting from contraction of three Gaussian primitives while the f-functions are contractions of four primitives. We refer to this basis set as basis set "AE", and we have improved this basis set in two ways. The last basis function of each type was decontracted and sets of polarization d-functions were added (indicated by an asterisk (*) in the basis descriptor). The resulting basis set is denoted (33333321/333321/3321*/31) in Huzinaga's nomenclature, and we refer to it as the all-electron double-ζ plus polarization basis set AEDZ+P.[30] The topological electron density analysis was carried out at the RHF/AEDZ+P//RHF/LANL1DZ+P level.

Computational Details. The ab initio calculations were carried out with Gaussian94[31] and earlier versions on a cluster of IBM RS-6000 systems and a Silicon Graphics PowerChallenge L computer. The program EXTREME was employed to determine the molecular graph of the total electron density function.[32] The natural bond orbital (NBO) analysis employed the NBO module[33] embedded in the Gaussian program. The 3-dimensional contour plots of the partial electron density functions $\rho_{PED}(x,y,z)$ were generated with the programs[34] PSICON and PSI2/88 which were adapted to contour electron density functions (rather than molecular orbitals) that were described by a 3-dimensional matrix of $\rho_{PED}(x,y,z)$ values computed with the program[35] Netz3D.

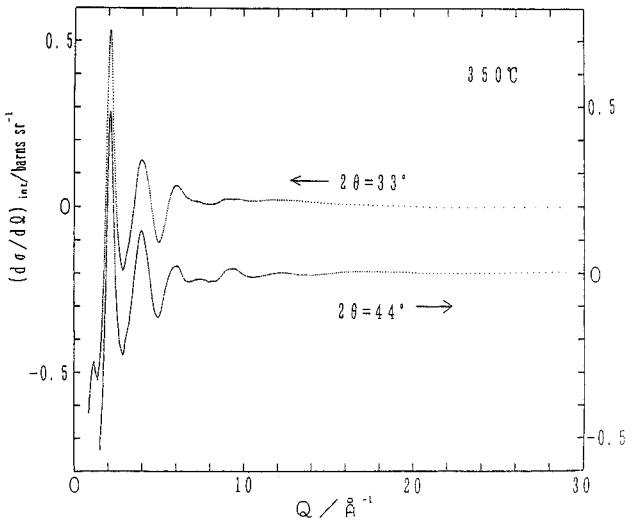

Figure 1. $2\theta = 33°$ and 44°. All measurements were carried out at 350 ± 5 °C.

Analyses and Discussion of the Neutron Diffraction of Bi_5^{3+} in the Liquid State

Time-of-flight neutron scattering from Bi_5^{3+} has been measured for molten $Bi_5(AlCl_4)_3$ in the liquid state to determine the intramolecular structures of the ions Bi_5^{3+} and $AlCl_4^-$ and of their intermolecular aggregation. The observed interference cross sections, as defined by eq 1, for the detectors at the scattering angles 33° and 44° and at 350 ± 5 °C are shown in Figure 1.

The radial distribution functions RDF(r) defined by eq 6 were obtained from the Fourier transform of the interference term observed at both 350 and 450 °C, as shown in Figure 2. There are no separate or isolated peaks located in the RDF(r) that would correspond to the intramolecular distances of D_{3h}-Bi_5^{3+} (Chart 1). This is due to the large magnitude of the intramolecular contributions of the complex ion $AlCl_4^-$. In order to get $RDF^{rem}(r)$ without any intramolecular contributions of $AlCl_4^-$, the term of $(d\sigma/d\Omega)_{int}^{intra}$ just for this complex ion has been estimated with eq 4. In previous work, $r_{AlCl} = 2.18$Å,

(23) (a) Pople, J. A.; Head-Gordon, M.; Raghavachari, K. *J. Chem. Phys.* **1987**, *87*, 5968. (b) Pople, J. A.; Head-Gordon, M.; Raghavachari, K. *J. Chem. Phys.* **1989**, *90*, 4635.
(24) Purvis, G. D.; Bartlett, R. J. *J. Chem. Phys.* **1992**, *76*, 1910.
(25) For a recent discussion of the accuracy of QCISD methods, see: He, Z.; Kraka, E.; Cremer, D. *Int. J. Quantum Chem.* **1996**, *57*, 157.
(26) Wadt, W. R.; Hay, P. J. *J. Chem. Phys.* **1985**, *82*, 284.
(27) *Gaussian Basis Sets for Molecular Calculations*; Huzinaga, S., Ed.; Elsevier: New York, New York, 1984; (a) p 23 ff, (b) p 379 ff.
(28) All calculations with the LANL1DZ+P basis set were carried out using the general basis set input option in Gaussian92. The addition of the polarization functions via modification of the internally stored basis set (keyword massage) produces inaccurate electrical moments.
(29) Stevens, W. J.; Krauss, M.; Basch, H.; Jasien, P. G. *Can. J. Chem.* **1992**, *70*, 612.
(30) The total energy of the ^{4}S state of Bi is −20 041.810 394 au at ROHF/AEDZ+P, and it is −20 041.665 360 au at the ROHF/AE level. Note that the latter value is 0.11 mhartrees lower than the published value.
(31) Frisch, M. J.; Trucks, G. W.; Schlegel, H. B.; Gill, P. M. W.; Johnson, B. G.; Robb, M. A.; Cheeseman, J. R.; Keith, T.; Petersson, G. A.; Montgomery, J. A.; Raghavachari, K.; Al-Laham, M. A.; Zakrzewski, V. G.; Ortiz, J. V.; Foresman, J. B.; Cioslowski, J.; Stefanov, B. B.; Nanayakkara, A.; Challacombe, M.; Peng, C. Y.; Ayala, P. Y.; Chen, W.; Wong, M. W.; Andres, J. L.; Replogle, E. S.; Gomperts, R.; Martin, R. L.; Fox, D. J.; Binkley, J. S.; Defrees, D. J.; Baker, J.; Stewart, J. P.; Head-Gordon, M.; Gonzalez, C.; Pople, J. A. *Gaussian94*, Revision C.3; Gaussian, Inc.: Pittsburgh, PA, 1995.
(32) EXTREME: Biegler-König, F. W.; Bader, R. F. W.; Tang, T. H. *J. Comput. Chem.* **1982**, *3*, 317.
(33) Glendening, E. D.; Reed, A. E.; Carpenter, J. E.; Weinhold, F. NBO 3.0; Theoretical Chemistry Institute and Department of Chemistry, University of Wisconsin: Madison, WI, 1990.
(34) PSICON and PSI2/88 by Severance, D. L., and Jorgensen, W. L., Department of Chemistry, Purdue University, West Lafayette, IN.
(35) Netz3D by Glaser, R., University of Missouri−Columbia, Columbia, MO, 1990.

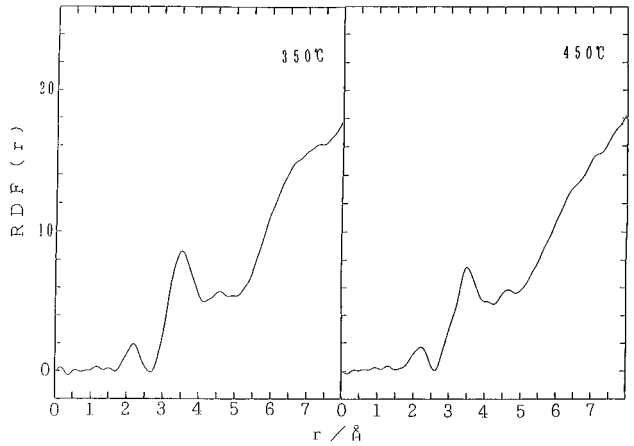

Figure 2. The radial distribution functions RDF(r) at 350 °C (left) and 450 °C (right).

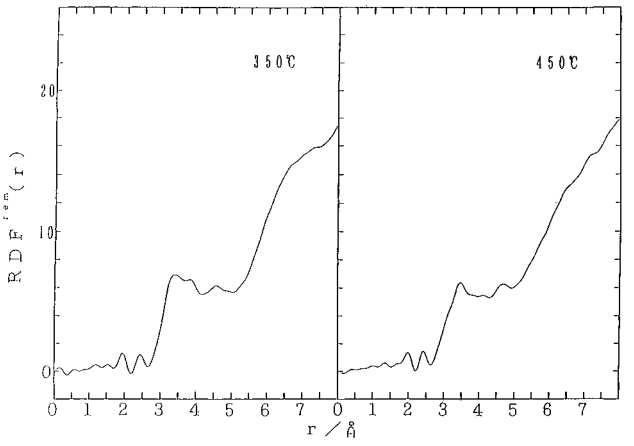

Figure 3. The remaining radial distribution functions RDF^{rem}(r) at 350 °C (left) and 450 °C (right).

r_{ClCl} = 3.57 Å, l_{AlCl} = 0.16 Å, and l_{ClCl} = 0.22 Å were determined by a least-squares fit to the interference term for molten $LiAlCl_4$, which includes no lithium contribution, recorded above 5 Å by the detectors set at scattering angles of about 150°.[36] The Fourier transform of $(d\sigma/d\Omega)_{int}^{rem}$ obtained by the subtraction of the intramolecular term eq 4 from the observed $(d\sigma/d\Omega)_{int}$ gives RDF^{rem}(r), as shown in Figure 3, at 350 and 450 °C. Since the partially separated peak around 3.5Å in RDF^{rem}(r) of Figure 3 includes no large contribution of the correlation between Cl and Cl in $AlCl_4^-$, it should become useful to determine the intramolecular structure of Bi_5^{3+} (D_{3h}) in the liquid state.

The First Sharp Diffraction Peak (FSDP). The FSDP in the observed $(d\sigma/d\Omega)_{int}$ of molten $Bi_5(AlCl_4)_3$ is located at ca. 1.2 $Å^{-1}$ (Figure 1). It can be understood in terms of (1) the layer structure in the glassy state,[37] (2) an intermediate range order (IMRO) in the packing among structural units having a size of about 5 Å in diameter,[37−39] and (3) the zone of low atomic occupancy or interstitial volume around cation-centered structural units or clusters.[40] The observed FSDP at ca. 1.2 $Å^{-1}$ suggests that the interatomic distance between unlike ions Bi_5^{3+} and $AlCl_4^-$ is equal to ca. 5.5 Å in molten $Bi_5(AlCl_4)_3$ according to the above models 2 or/and 3. This is a reasonable model since the crystal structure for $Bi_5(AlCl_4)_3$ exhibits interatomic distances between the center of mass of Bi_5^{3+} and the nucleus of Al in $AlCl_4^-$ that lie within the range 5.6−6.2 Å.

Model of Intermediate Range Order (IMRO) and Simulation of the Observed RDF^{rem}(r). The IMRO should be established also in the liquid state because of the observed FSDP: The local configuration around Bi_5^{3+} may in principle be similar to the configuration of the 12 complex ions of $AlCl_4^-$ around a homopolyatomic bismuth ion of Bi_5^{3+} in the crystalline phase. The functions RDF^{rem}(r) (Figure 3) measured at 350 and 450 °C have been simulated up to ca. 5 Å by a model of IMRO similar to the configuration of the 12 complex ions of $AlCl_4^-$ around Bi_5^{3+} in the crystal structure of $Bi_5(AlCl_4)_3$ (Chart 2). This model shows (1) the six correlations between a capping or axial Bi atom (Bi_a) and a base or equatorial Bi atom (Bi_e),

Chart 2

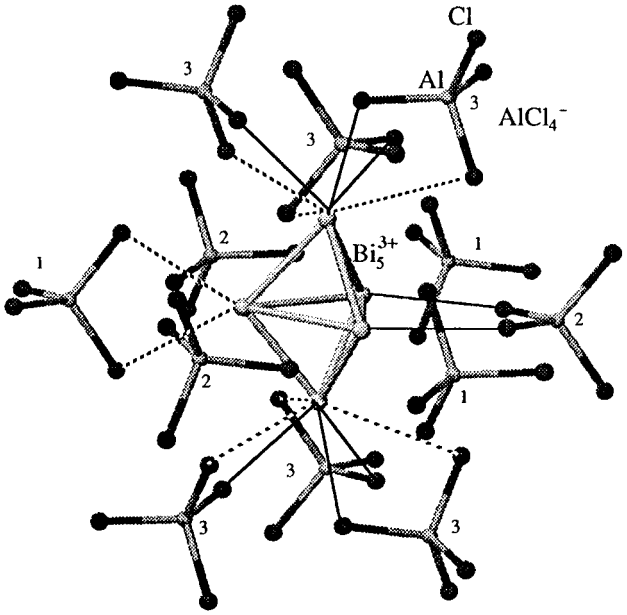

[a] There are three types of Bi−Cl contacts (indicated by numbers 1, 2, and 3), and they give rise to two different Bi−Cl distances, represented by solid and dashed lines (see text) in the IMRO.

which are due to Bi_5^{3+} (D_{3h}) and are separated by $3.1_5 \pm 0.05$ Å, and (1′) the three correlations between two Bi_e's, which are separated by $3.4_0 \pm 0.05$ Å in Bi_5^{3+}, (2) the 12 correlations between Bi and Cl (pairs identified by solid lines in Chart 2), which are separated from each other by the first nearest neighbor distance of $3.7_5 \pm 0.05$ Å, and (2′) the 12 correlations between Bi and Cl (pairs identified by dashed lines in Chart 2), which are separated from each other by the second nearest neighbor distance of $4.2_0 \pm 0.05$ Å, and (3) the 24 correlations between Al and Bi, which are separated from each other by $4.5_5 \pm 0.05$ Å (Figure 4). After melting of the solid $Bi_5(AlCl_4)_3$ the distances of Bi_a-Bi_e and Bi_e-Bi_e show increments of 0.1_5 and 0.2_0 Å and the interatomic distances of Bi_a-Cl/Bi_e-Cl and Bi_a-Al/Bi_e-Al show increases of 0.3_0 and 0.5_0 Å. The plots in Figure 4 show that the intramolecular distances of Bi_5^{3+} (D_{3h}) in the liquid state are independent of temperature within experimental uncertainty and the intermolecular distances become about 0.1 Å longer at the higher temperature of 450 °C compared to 350 °C. Figure 4 demonstrates in a compelling fashion the success of the simulation according to the above

(36) Kameda, Y.; Ichikawa, K. *J. Chem. Soc., Faraday Trans.* **1987**, *83*, 2925.
(37) Price, D. L.; Moss, S. C.; Reijers, R.; Saboungi, M-L.; Susman, S. *J. Phys. Condens. Matter* **1989**, *1*, 1005.
(38) Ichikawa, K.; Kameda, Y.; Xu, Q.; Misawa, M. *J. Non-Cryst. Solids* **1987**, *95/96*, 185.
(39) Ichikawa, K. *J. Phys. Condens. Matter* **1995**, *7*, L135.
(40) Elliott, S. R. *Phys. Rev. Lett.* **1991**, *67*, 711.

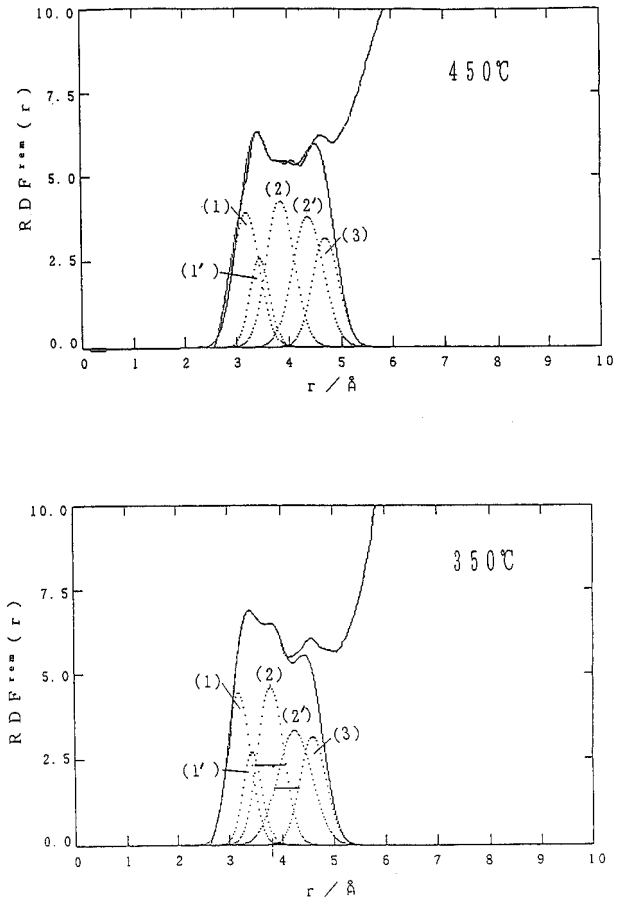

Figure 4. The simulation of $RDF^{rem}(r)$ at 350 °C (lower) and 450 °C (upper) by a model of the IMRO, as shown in Chart 2. The numbers in parentheses are explained in the text.

model of IMRO, which includes the 12 ions of $AlCl_4^-$ and a homopolyatomic bismuth ion of Bi_5^{3+}.

Ab Initio Electronic Structure Analysis of the Bi_5^{3+} Ion

Since the neutron diffraction of a liquid does not have sufficiently high resolution to determine a reasonable intramolecular electron density distribution $\rho(x,y,z)$ of Bi_5^{3+}, we have estimated the electron density distributions with the aid of modern ab initio molecular orbital theory. However, one must recognize that the ab initio calculations model the isolated Bi_5^{3+} ion, whereas the neutron diffraction clearly shows the Bi_5^{3+} ions to be stabilized by an environment of complex ions of $AlCl_4^-$. Moreover, the ab initio calculations predict structures at 0 K while the diffraction experiment was carried out at about 700 K. The methodological differences are substantial and need to be kept in mind in comparative analyses. This realization stresses that one should not be satisfied with a theoretical model on the grounds that it "predicts" the condensed phase structure. Rather one must always use the very best theoretical levels possible and the comparison between theory and experiment should then be used to make deductions as to environmental effects on structure.

Potential Energy Surface Analysis. Geometries were optimized at the RHF, MP2, and QCISD(T) levels using the basis sets LANL1DZ, LANL1DZ+P, and LANL1DZ+PP. The results are summarized in Table 1. The stationary structures obtained at the RHF and MP2 levels were confirmed and fully characterized via the computation of first and second derivatives. The D_{3h} structure corresponds to a minimum at all levels of theory employed. Irrespective of the basis set used, the correlated methods MP2 and QCISD(T) favor slightly lower Δ(Bi−Bi) values, that is, a longer and slimmer bipyramid, as compared to the RHF method, and this effect is consistently overestimated by the MP2 method. In comparison to the Bi_e−Bi_e distances, the nearest neighbor distances Bi_a−Bi_e are shorter by about 0.2−0.3 Å at all of the levels of ab initio theory that employ polarized basis sets, by ca. 0.3 Å in the case of the $Bi_5(AlCl_4)_3$ crystal, and by ca. 0.2_5 Å for its liquid. With regard to this intramolecular structural feature there is qualitative agreement among isolated Bi_5^{3+} at 0 K, Bi_5^{3+} surrounded by $AlCl_4^-$ complex ions in the solid state at 300 K, and Bi_5^{3+} surrounded by gegenions in the liquid phase at ca. 700 K. Hence, we conclude that this structural feature is an intrinsic property of the tripositive ion.

As far as absolute bond lengths are concerned, it can be seen that the addition of polarization functions shortens all Bi−Bi bonds by 0.1−0.2 Å and the effect is slightly more pronounced for the Bi_e−Bi_e bond. The optimization of the d-exponent through linear combination has a noticeable albeit much smaller structural effect. The computed structures are the equilibrium structures in the harmonic approximation, and they should be a lower limit to the true structures at 0 K. Anharmonicities and thermal motion both would lengthen the bonds. Hence, the QCISD(T) structures computed with either of the polarized basis sets overestimate the bond lengths slightly, but the agreement with experiment is still excellent.

Natural Population Analysis of Bi_5^{3+}. The atomic charges derived by the natural population analysis (NPA) are summarized in Table 2 together with the ratio of the charges on the equatorially and axially placed Bi atoms, Bi_e/Bi_a, and the PTC_e values which specify the total charge on the Bi atoms as a percentage of the total positive charge. Independent of the theoretical level, we find that the charge on the axial Bi atoms (+0.74) is much larger than the charge on the equatorial atom (+0.51, $Bi_e/Bi_a \approx 0.7$). This feature might reflect that equatorial Bi atoms are involved in four Bi−Bi bonds while axial Bi atoms are engaged in three Bi−Bi bonds only. Electron density on equatorial Bi atoms is more beneficial to bonding stabilization. The NPA data coincide rather well with the Mulliken charges reported by Ulvenlund et al.,[19] and in fact, this coincidence is both surprising and fortuitous considering that Mulliken's approximation of equal partitioning of the overlap populations cannot be expected to hold for polar bonds. The overall resulting motif indicated by these atom populations essentially consists of an equal distribution of charge over the sets of axial and equatorial atoms ($PTC_e \approx 50\%$). Note that the computed charges are not what one would expect considering that the Bi_e−Bi_e distances exceed the Bi_a−Bi_e distances.

Cluster Molecular Orbitals and Partial Electron Density Functions. The "natural electron configurations" defined by the NBO method provide a framework for the assignment of the total natural charge of an atom to various components of the atoms' atomic orbitals. The data show only modest removal of electron density from the 6s-AO. The natural localized orbitals indicate that lone pairs are present on all Bi atoms and these lone pairs are essentially of s-character. Hence, the differences in the atom populations reflect different degrees of removal of electron density from the p-AOs of the equatorial and axial Bi atoms which are involved in cluster bonding. This finding corroborates and validates the 6s−6p and 6s−6d separations made in Corbett's semiempirical treatment (*vide supra*).[12] Thus, the bonding in the ion can be approximated well by consideration of the cluster orbitals that result from interaction of the Bi p-AOs. The cluster MOs that result from capping the trigonal base by two axial Bi atoms can be constructed as shown in Chart 3.[41,42] The orbitals due to the

Table 1. Structures of D_{3h}-Symmetric Bi_5^{3+} Ions[a]

method	Bi_a-Bi_e	Bi_e-Bi_e	$X-Bi_a$	$X-Bi_e$	$\Delta(Bi-Bi)$[b]
X-ray diff, single crystal[c]	3.007(2)	3.318(62)			0.311
X-ray diff, single crystal[d]	3.013(5)	3.326(6)			0.313
neutron diff, single crystal[c]	3.01	3.32			0.31
neutron diff, melt	3.2	3.4			0.2
RHF/LANL1DZ	3.0949	3.4732	2.3574	2.0053	0.38
MP2/LANL1DZ	3.2030	3.4654	2.5013	2.0008	0.26
QCISD(T)/LANL1DZ	3.2131	3.5484	2.4753	2.0487	0.34
RHF/LANL1DZ+P	2.9985	3.3093	2.3110	1.9106	0.31
MP2/LANL1DZ+P	3.0565	3.2435	2.4156	1.8726	0.19
QCISD(T)/LANL1DZ+P	3.0657	3.3092	2.3975	1.9106	0.24
RHF/LANL1DZ+PP	3.0120	3.3406	2.3135	1.9287	0.33
MP2/LANL1DZ+PP	3.0598	3.2550	2.4146	1.8793	0.20
QCISD(T)/LANL1DZ+PP	3.0726	3.3311	2.3963	1.9232	0.26

[a] All distances in angstroms. [b] $\Delta(Bi-Bi) = d(Bi_e-Bi_e) - d(Bi_a-Bi_e)$. [c] $Bi_5(AlCl_4)_3$. Krebs et al., ref 14. [d] $Bi_5(GaCl_4)_3$. Ulvenlund et al., ref 19.

Table 2. Natural Population Analysis

theoretical level	Bi_e	Bi_a	Bi_e/Bi_a	PTC_e
RHF/LANL1DZ	+0.527	+0.709	0.743	52.7
MP2/LANL1DZ	+0.508	+0.738	0.688	50.8
QCISD/LANL1DZ	+0.524	+0.713	0.734	52.4
RHF/LANL1DZ+P	+0.522	+0.718	0.727	52.2
MP2/LANL1DZ+P	+0.484	+0.775	0.625	48.4
QCISD/LANL1DZ+P	+0.504	+0.744	0.677	50.4
RHF/LANL1DZ+PP	+0.530	+0.704	0.753	53.0
MP2/LANL1DZ+PP	+0.484	+0.774	0.625	48.4
QCISD/LANL1DZ+PP	+0.509	+0.736	0.692	50.9

[a] The PTC_e values specify the total charge on the equatorial Bi atoms in percent of the total positive charge which is equivalent to $100q(Bi_e)$. [b] QCISD densities computed with the QCISD(T) optimized structures.

base and capping atoms, respectively, are shown to the left and right, and orbital interactions are considered separately for radial and of two sets of tangential p-AOs. Radial AOs are directed inward, and tangential AOs are either parallel or perpendicular with respect to the main axis. The MOs resulting from LCAO of the radial p-AOs are easily constructed, and there is only one bonding MO of a_1' symmetry. LCAO of the antibonding combination of parallel AOs of the axial Bi atoms with the a_2'' base combination leads to a strongly bonding a_2''-MO. The perpendicular p-AOs result in a pair of e′-MOs. Finally, one needs to consider that the antibonding set of parallel base orbitals may interact with the antibonding combination of the perpendicular axial p-AOs. This interaction causes a set of e″-MOs to be lowered, and as will be seen later, the resulting e″-MOs are in fact lowered below the e′-MOs. Thus, the lowest-lying cluster MOs for skeletal bonding of the trigonal bipyramid are a_1' (radial), e″ (mixed), a_2'' (||), and e′(⊥).

If the wave function Ψ is described by a single Slater determinant, then the electron density distribution $\rho_{mol}(x,y,z)$ can be expressed as a sum over the squares of all of the occupied molecular orbitals $\psi_i(x,y,z)$; $\Psi = \Sigma_{occ}|\psi_i(x,y,z)|^2$. The quantity $\rho_i(x,y,z) = |\psi_i(x,y,z)|^2$ represents the partial electron density function (PED) due to MO ψ_i. We computed the partial electron density distribution functions associated with the six highest occupied molecular orbitals for Bi_5^{3+}, and contour plots are shown in Figure 5. The remaining five of the 11 valence orbitals result from LCAOs of Bi s-AOs, and these MOs all have the

Chart 3. Construction of the Cluster Molecular Orbitals That Result from Capping the Trigonal Base by Two Axial Bi Atoms

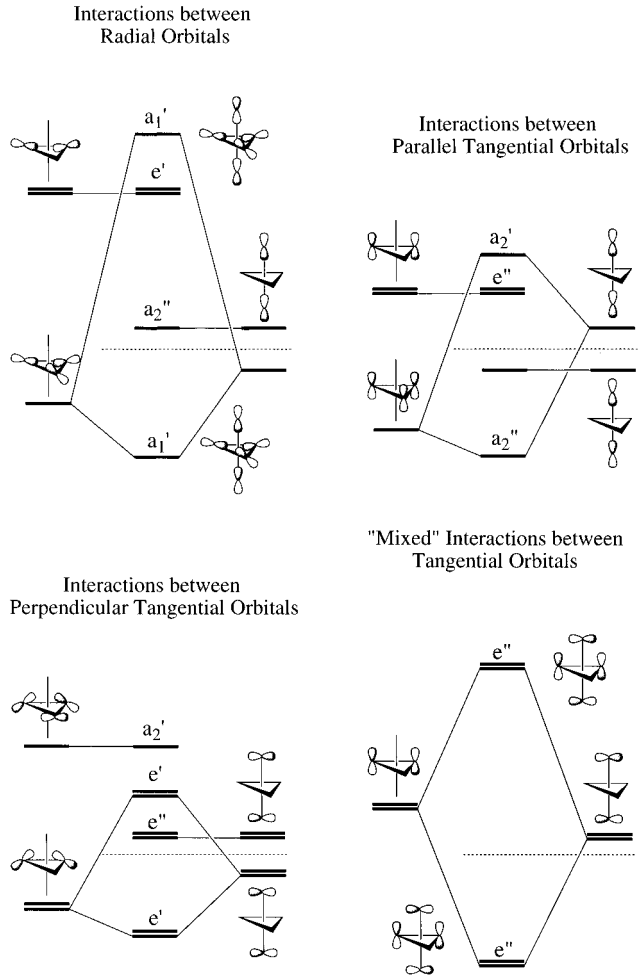

expected shapes. The cluster orbitals derived schematically for the D_{3h} isomer are easily recognized, and there are only minor qualitative differences. The a_1' cluster orbital, for example, is found to have more contributions from the Bi_e than from the Bi_a atoms. One of the advantages provided by the partial electron density functions lies with degenerate sets of MOs. For degenerate sets of MOs, only their combination can be assigned significance and this combination can easily be visualized via the partial electron density $\rho_e(x,y,z) = |\psi_{e,1}(x,y,z)|^2 + |\psi_{e,2}(x,y,z)|^2$. In Figure 6, the two sets are shown of the e′- and e″-symmetric MOs together with the plots of the functions $\rho_{e'}$-

(41) (a) Albright, T. A.; Burdett, J. K.; Whangbo, M.-H. *Orbital Interactions in Chemistry*; John Wiley & Sons: New York, 1985; p 426 ff. (b) The dashed lines in Chart 3 indicate the nonbonding level in a neutral system of this type. In the tripositive ion, all of these and many of the virtual MOs are of course strongly bonding.
(42) Stone, A. J. *Inorg. Chem.* **1981**, *20*, 503.

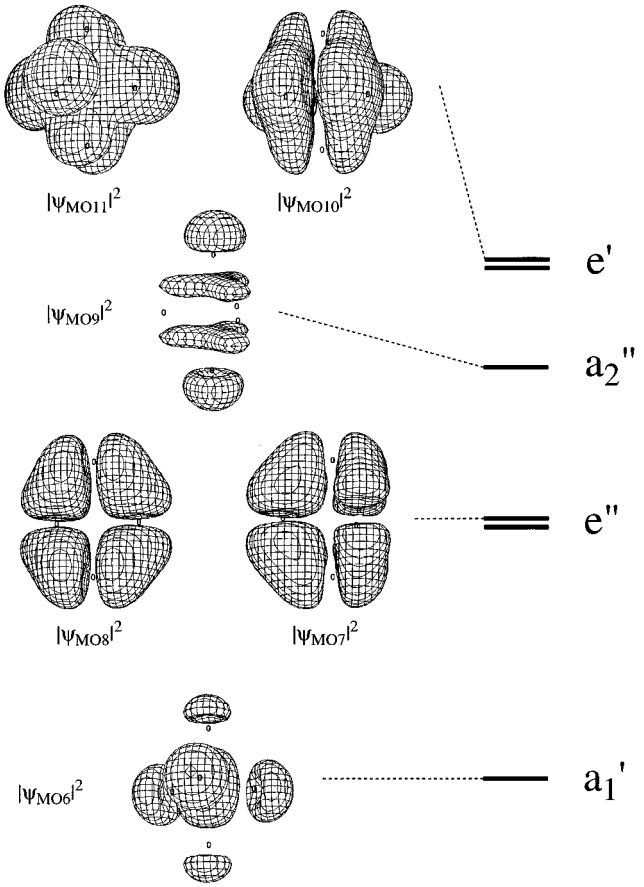

Figure 5. Contour plots of the partial electron density functions $\rho_{PED}(x,y,z)$ associated with the cluster orbitals of D_{3h}-symmetric Bi_5^{3+}. The energy levels are drawn to scale.

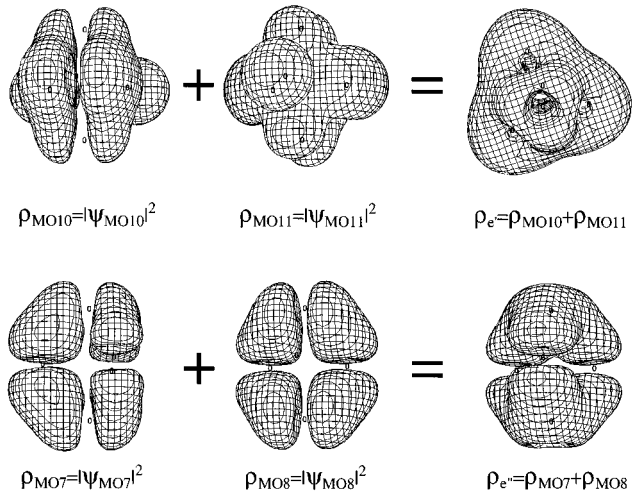

Figure 6. The combination of the partial electron density functions of the MOs of each e-symmetric set resulting in the partial electron densities $\rho_{e'}$ and $\rho_{e''}$ with the appropriate overall symmetry.

(x,y,z) and $\rho_{e''}(x,y,z)$. Only the partial electron density functions reflect the C_3 symmetry, as is well illustrated in Figure 6. Furthermore, the plots of $\rho_{e'}(x,y,z)$ and $\rho_{e''}(x,y,z)$ show very clearly that the e′ and e″ sets, respectively, are responsible primarily for Bi_e-Bi_e and Bi_e-Bi_a bonding.

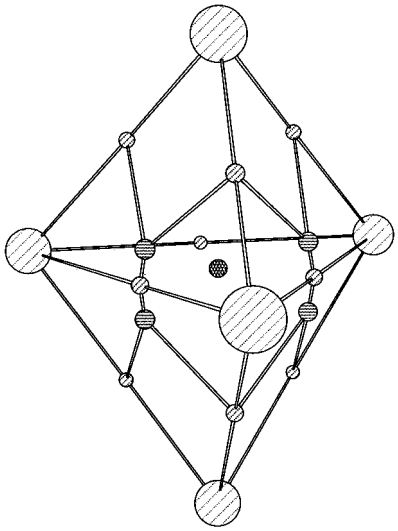

Figure 7. The molecular graph of D_{3h}-Bi_5^{3+}. All atoms and critical points are shown at their exact locations. Bond paths are shown schematically as straight lines, and in addition, connecting lines have been drawn between ring critical points and adjacent bond critical points. (The two ring critical points of the triangles on the "backside" of the molecule are not shown for clarity of the presentation.)

Molecular Graph of the Bi_5^{3+} Ion. The topological electron density analysis involves the characterization of the electron density distribution based on properties of the gradient vector field. The details of this analysis will be described elsewhere, and we will focus here on a brief description of the molecular graph (Figure 7). The collection of all gradient vector field lines originating at a given atom, the attractor, define the associated zero-flux surfaces as the boundaries of the atoms in the molecules. Bond critical points occur at the intersection between the zero-flux surfaces and the so-called bond paths. A bond path connects two attractors and is defined as the line traced out by following the direction of positive curvature of the electron density beginning at the bond critical point. One locates all bond critical points and then traces out the zero-flux surfaces following the directions associated with the two negative principal curvatures of the density. We also traced out the bond paths to measure their lengths and found them to be rather straight. The molecular graph of the D_{3h}-symmetric cluster shows the expected characteristics (Figure 7). Bond paths occur along all edges of the bipyramid, ring points exist in the center of each face, and there exists a cage point in the center of the tripositive cation.

Acknowledgment. This research was supported by a Grant-in-Aid (No. 07236201) from the Ministry of Education, Science, and Culture. Part of this research was carried out while R.G. was visiting Japan as a fellow of the Japan Society for the Promotion of Science (JSPS) in the summer of 1997.

IC970608H